JARA: 'Just Another Red list Assessment'

Henning Winker[1,2] *& Richard B. Sherley*[3]

[1] Department of Agriculture, Forestry and Fisheries (DAFF), Roggebaai, 8012 Cape Town, South Africa
[2] Centre for Statistics in Ecology, Environment and Conservation (SEEC), Department of Statistical Sciences, University of Cape Town, South Africa.
[3] Environment and Sustainability Institute, College of Life and Environmental Sciences, University of Exeter, Penryn Campus, Cornwall, TR10 9FE, UK

Correspondance: Henning Winker. E-mail: henning.winker@gmail.com; Richard B. Sherley. Email: r.sherley@exeter.ac.uk.

Abstract

Identifying species at risk of extinction is necessary to prioritise conservation efforts. The International Union for Conservation of Nature's (IUCN) Red List of Threatened Species is the global standard for quantifying extinction risk, with many species categorised on the basis of a reduction in population size (Criterion A). We introduce the Bayesian state-space framework 'JARA' (Just Another Red-List Assessment). Designed as an easy to use, rapid and widely applicable decision-support tool, JARA allows both process error and uncertainty to be incorporated into IUCN Red List assessments under criterion A. A key output of JARA is an easy to interpret graphic in which the probability distribution of the population decline is displayed against the IUCN Red List categories, where each category is assigned a probability given process and observation uncertainty. We provide fully commented R code on the global open-source platform GitHub (https://github.com/henning-winker/JARA), so that JARA can be modified and applied by conservation practitioners to their own count or relative abundance data. We illustrate the application of JARA using two real-world examples: (i) relative abundance indices from scientific trawl surveys for two elasmobranchs, Yellowspotted Skate *Leucoraja wallacei* and Whitespot smoothhound *Mustelus palumbes*; and (2) absolute abundance data (census counts) from the global Cape Gannet *Morus capensis* population.

Background

Quantifying trends in population abundance is central to ecological research and to conservation biology in particular, where identifying species at risk of extinction is necessary to prioritise effort

in the face of ever-increasing biodiversity loss (Butchart et al., 2004; Hoffmann et al., 2008). Although a number classification protocols exist to assess a species' extinction risk (Regan et al., 2013), the International Union for the Conservation of Nature's (IUCN) Red List of Threatened Species is viewed widely as the global standard (Hoffmann et al., 2008; Mace et al., 2008).

To list a species in a threatened category (vulnerable [VU], endangered [EN] or critically endangered [CR]) on the Red List, assessors can consider the risks associated with both the small-population paradigm and the declining population paradigm (Caughley, 1994) under five assessment criteria (A to E). However, quantitative information on species abundance – as a direct measure of the status of a population – is often preferred over less direct measures of extinction risk, like changes in habitat extent or quality (Mace et al., 2008; Wilson, Kendall, & Possingham, 2011). Moreover, the IUCN guidelines allow for assignment to a category (ranging from Least Concern [LC] to Extinct) based only on the criterion that produces the highest estimated risk (Mace et al., 2008). Therefore, species are often listed only on the basis of a reduction in population size (Criterion A); as of today > 5,000 species are classified as threatened on this basis alone (Rueda-Cediel, Anderson, Regan, & Regan, 2018). Criterion A is thus considered to be the most widely used stand-alone criterion for assigning a Red List status to a wide range of animal taxa, including mammals, birds, reptiles, fishes and insects (Butchart et al., 2004; Dulvy, Jennings, Rogers, & Maxwell, 2006; Mace et al., 2008; Seminoff & Shanker, 2008; Fox et al., 2018).

Bayesian implementations of state-space models offer a powerful framework to improve the characterization and communication of uncertainty during IUCN Red List assessments. The posterior probabilities provide an intuitive and transparent way of expressing uncertainty about population declines to conservation practitioners (Bauer et al., 2015; Sherley et al., 2018), which can be translated directly into probabilistic statements about a population falling into a threatened category (Bauer et al., 2015; Boyd et al., 2017). However, developing customized Bayesian state-space models can be technically demanding and time consuming. This can be aggravated when dealing with often case-specific, 'messy' abundance data that are subject to missing values, irregular spacing or multiple indices that are measured at different scales. These issues may therefore dissuade some conservation practitioners and hamper broader applications.

To address this, we have developed the Bayesian state-space framework 'JARA' (Just Another Red-List Assessment). Designed as an easy to use, rapid and widely applicable decision-support tool, JARA allows both process error and uncertainty to be incorporated into Red List assessments. A key output of JARA is an easy to interpret graphic in which the probability distribution of the population decline is displayed against the IUCN Red List categories, where each category is assigned a probability given process and observation uncertainty. To ensure a high degree of transparency and reproducibility, we provide fully commented R code on the global open-source platform GitHub (https://github.com/henning-winker/JARA), so that JARA can be modified and applied by conservation practitioners to their own count or relative abundance data.

We illustrate the application of JARA using simulations and two real-world examples: (i) relative abundance indices from scientific trawl surveys for two elasmobranchs, Whitespot smoothhound *Mustelus palumbes* (Figure 1, top panel) and Yellowspotted Skate *Leucoraja wallacei* (Figure 1, middle panel) and; and (2) absolute abundance data (census counts) from the global Cape Gannet *Morus capensis* population (Figure 1, bottom panel).

The JARA modelling frame work

JARA represents a generalized Bayesian state-space decision-making tool for trend analysis of abundance indices with direct applications to IUCN Red List assessments. The name 'Just Another Red List Assessment' acknowledges JAGS (Just Another Gibbs Sampler, Plummer, 2003), which is the software called from R to run the Bayesian state-space model application. The name reference, together with user-friendly R interface and modulated coding structure of JARA follows the example of the new open source fisheries stock assessment software 'Just Another Bayesian Biomass Assessment' (JABBA; Winker, Carvalho, & Kapur, 2018). JARA enables analysis of one or multiple abundance indices simultaneously, where each index can contain missing years and span different periods. JARA provides the option for fitting relative abundance indices to estimate a mean trend or absolute abundance indices (from e.g. different subpopulations) to produce a summed population trend for the total population.

State-Space Model Formulation

A central assumption of the state-space approach is that the abundance (I_t) trend follows a Markovian process, such that I_t in year *t* will be conditioned on I_{t-1} in the previous year *t*. For generality it is assumed that the underlying population trend follows a conventional exponential growth model $I_{t+1} = I_t\lambda_t$ (e.g. Kery & Schaub, 2012), where λ_t is the growth rate in year *t*. The growth rate λ_t is allowed to vary annually to accommodate fluctuations in reproductive success and survival as a result of environmental conditions, anthropogenic mortality or other latent (unobservable) impacts. State-space models are hierarchical models that explicitly decompose an observed time-series into a process variation and an observation error component (Simmons et al., 2015). On the log scale, the process equation becomes $\mu_{t+1} = \mu_t + r_t$, where $\mu_t = \log(I_t)$ and $r_t = \log(\lambda_t)$ is the year-to-year rate of change, with variations in log-growth rates following a random normal walk $r_t \sim Normal(\bar{r}_p, \sigma_\eta^2)$, given the estimable process error variance σ_η^2 and the estimable mean population rate of change $\bar{r}_p$ (i.e. the underlying trend). The corresponding observation equation is of the form $\log(y_t) = \mu_t + \epsilon_t$, where y_t denotes the abundance value for year *t*, ϵ_t is observation residual for year *t*, which is assumed to be normally distributed on log-scale $\varepsilon_t \sim Normal(0, \sigma_\varepsilon^2)$ as a function of the observation variance σ_ε^2.

The model notation for relative abundance indices builds on the Bayesian state-space tool for averaging relative abundance indices by Winker *et al*. (2018). This is based on the assumption that the mean underlying abundance trend is an unobservable state variable. The corresponding observation equation is then modified, such that $\log(y_{t,i}) = \mu_t + \log(q_i) + \epsilon_{t,i}$, where $y_{t,i}$ is the relative abundance value for year *t* and index *i,* μ_t is the natural logarithm of the mean abundance trend, $\varepsilon_{t,i}$ is the lognormal observation error term for index *i* and year *t*, and q_i is a scaling parameter for index *i.* The abundance index with the oldest record (in order of occurrence) is taken as a reference index by fixing $q_1 = 1$ and the other indices are scaled to this reference index, respectively, with $q_{2,\ldots,n}$ being estimable model parameters. The estimated posterior of the population trend for year *t* is then given by $I_{p,t} = \exp(\mu_t)$.

To estimate a total abundance trajectory for the "global" population from multiple absolute abundance indices, we assume that each absolute abundance index represents a 'subpopulation'

that may increase or decline independently from other subpopulations. The process equation is therefore modified to $\mu_{t,i} = \mu_{t,i} + r_{t,i}$, where $r_{t,i} = \log(\lambda_{t,i})$ is the year-to-year rate of change specific to index *i* that is assumed to vary around $\bar{r}_i$ to represent the underlying mean rate of change for the subpopulation instead of a global population mean $\bar{r}_p$, but with a process variance σ_η^2 that is common to all subpopulations $r_{t,i} \sim Normal(\bar{r}_i, \sigma_\eta^2)$. The corresponding observation equation is adjusted to $\log(y_{t,i}) = \mu_{t,i} + \epsilon_{t,i}$, so that abundance trend $\mu_{t,i}$ and the error term $\varepsilon_{t,i} \sim Normal(0, \sigma_{\varepsilon_i}^2)$ now become the specific to subpopulation *i*. The estimated posterior of the global population trajectory $I_{p,t}$ for year *t* is then estimated from the sum of all individual subpopulation trajectory posteriors, such that $I_{p,t} = \sum_i \exp(\mu_{t,i})$.

Bayesian Framework

JARA is run from the statistical environment R (R Core Team, 2014) and executed in JAGS (Plummer, 2003), using a wrapper function from the R library 'r2jags' (Su & Yajima, 2012). The Bayesian posterior distributions are estimated by means of Markov Chain Monte Carlo (MCMC) simulation. In JAGS, all estimable hyper-parameters have to be assigned to a prior distribution. JARA uses vague (uninformative) prior distributions throughout, so all inferences are drawn from the information in the data. The estimation of annual growth rate deviates r_t, is implemented through hierarchical priors (Jiao, Hayes, & Corte, 2009), where r_t is informed by the population mean $\bar{r}_p$ for relative abundance indices and $r_{t,i}$ is informed by $\bar{r}_i$ for absolute abundance indices. Normal prior distributions of $N(0,1000)$ are assumed for both $\bar{r}_p$ or $\bar{r}_i$. The initial population size in the first year $I_{t=1,i}$ is drawn in log-space from a 'flat' normal distribution with the mean equal to the log of the first available count $y_{t=1,i}$ and a standard deviation of 1000. Priors for the process variance can be either fixed or estimated. If estimated (default), the process variance prior is implemented via a vague inverse-gamma distribution by setting both scaling parameters to 0.001 (Chaloupka & Balazs, 2007; Brodziak & Ishimura, 2012; Carvalho et al., 2014), which yields an approximately uniform prior on the log scale.

The user definable options for the observation variance follow Winker *et al*. (2018). Accordingly, the total observation variance σ_ε^2 can be separated into three components: (1) externally derived standard error estimates $\sigma_{SE_{y,i}}^2$ for each abundance index *i*, (2) a fixed input variance σ_{fix}^2 and (3)

estimable variance σ^2_{est}, where the prior for σ^2_{est} assumes an uninformative inverse-gamma distribution with both scaling parameters set to 0.001. All three variance components are additive in their squared form (Francis, Hurst, & Renwick, 2003), so the total observation variance for abundance index *i* and year *y* is: $\sigma^2_{\varepsilon_{y,i}} = \sigma^2_{SE_{y,i}} + \sigma^2_{fix} + \sigma^2_{est}$. Each variance component can be individually switched on or off by the user. Adding a fixed observation error to externally estimated standard errors is common practice to account for additional sampling error associated with abundance indices and also informs the process variance as a portion of total variance is assigned *a priori* to observation variance (Winker et al. 2018).

Estimating probabilities of population decline

A posterior probability for the percentage change (*C%*) associated with each abundance index can be conveniently calculated from the posteriors of $\hat{I}_{p,y}$, the model predicted population trajectory. If $\hat{I}_{p,y}$ represents a longer time span than the assumed three generation lengths (GL), *C%* is automatically calculated as the difference between a three-year average around the final observed data point T, and a three-year average around the year corresponding to $T - (3 \times GL)$ The year $T + 1$ is always projected to obtain a three-year average around *T* to reduce the influence of short-term fluctuations (Froese et al., 2017). When the span of $\hat{I}_t$ is < 3 × GL, JARA projects forward, by passing the number of desired future years without observations to the state-space model until $\hat{I}_t > (3 \times GL) + 2$. The projections for a single population or multiple subpopulations *i* are based on all possible posterior realizations of $r_{t,i}$ across all *T* years in the observed time series: $\tilde{r}_i = \frac{1}{T}\sum_{t=1}^{T} r_{t,i}$.

Model Diagnostics

To evaluate model fit, JARA provides the user with three plots. The first shows the observed and predicted abundance values for each time series together with the 95% posterior predictive credibility intervals (Figure 2, upper panels). The second shows fits to each individuals timeseries, as well as the 95% credible intervals (CI) derived from the observation variance $\sigma^2_{\varepsilon_{y,i}}$ (Figure 3). The third is a residual plot, which illustrates potential data conflict when fitting multiple time series (Winker et al. 2018) and includes: (1) colour-coded lognormal residuals of observed versus predicted abundance indices *i*, (2) boxplots indicating the median and quantiles of all residuals

available for any given year; the area of each box indicates the strength of the discrepancy between the abundance indices (larger box means higher degree of conflicting information), and (3) a loess smoother through all residuals which highlights systematically auto-correlated residual patterns (Figure 2, lower panels). In addition, the Root-Mean-Squared-Error (RMSE) and the deviance information criterion (DIC) are provided for the comparison of goodness-of-fit and model selection purposes respectively. Convergence of the MCMC chains is diagnosed using the 'coda' package (Plummer, Nicky Best, Cowles, & Vines, 2006), adopting minimal thresholds of $p = 0.05$ for Heidelberger and Welch (Heidelberger and Welch, 1992) and Geweke's (Geweke, 1992) diagnostics called from R.

JARA decision support plots

To facilitate Red List assessment decision-making, JARA automatically produces four key plots (Figures 4 and 5) for each input dataset showing: (1) the combined state-space model fit and 95% CI to the multiple time-series where relative abundance time-series are used (e.g. Figure 2, top panels) or the individual state-space models fits to each count dataset for absolute abundance indices (e.g. individual colony counts for Cape Gannet; Figure 5, top left panel); (2) the overall observed and projected (±95% CI) population trajectory over three GL (Figure 4, top panels and Figure 5, top right panel); (3) the median and posterior probabilities for the percentage annual population change calculated from all the observed data, and from each of the most recent 1 GL, 2 GL, and 3 GL (depending on the length of the observed time-series), shown relative to a stable population ($\%C = 0$) (Figure 5, bottom left panel); and (4) how the posterior distribution for the percentage change in abundance ($\%C$) over 3 GL aligns against the thresholds for the Red List categories (Least Concern LC, Near Threatened NT, Vulnerable VU, Endangered EN or Critically Endangered CR) under criteria A2–A4 (e.g. Figure 4 bottom panels) or under A1.

Figures

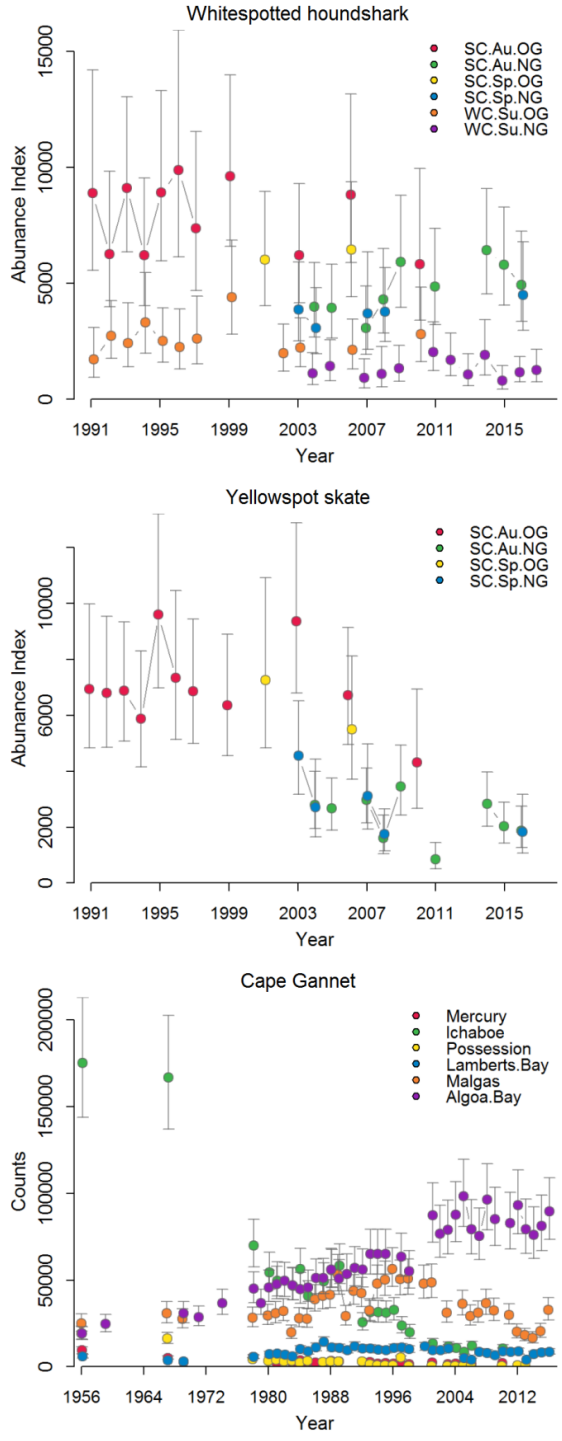

Figures 1: Input datasets of relative abundance indices from South African trawl surveys for two chondrichthyes species, Whitespot smoothhound *Mustelus palumbes* and (top) Yellowspotted Skate *Leucoraja wallacei* (middle) – both species are endemic to southern Africa and have been previously listed as Data Deficient – and for annual nest census (counts) data for Cape Gannets, *Morus capensis* – a large seabird endemic to the Benguela Ecosystem – from its six global breeding localities in Namibia and South Africa.

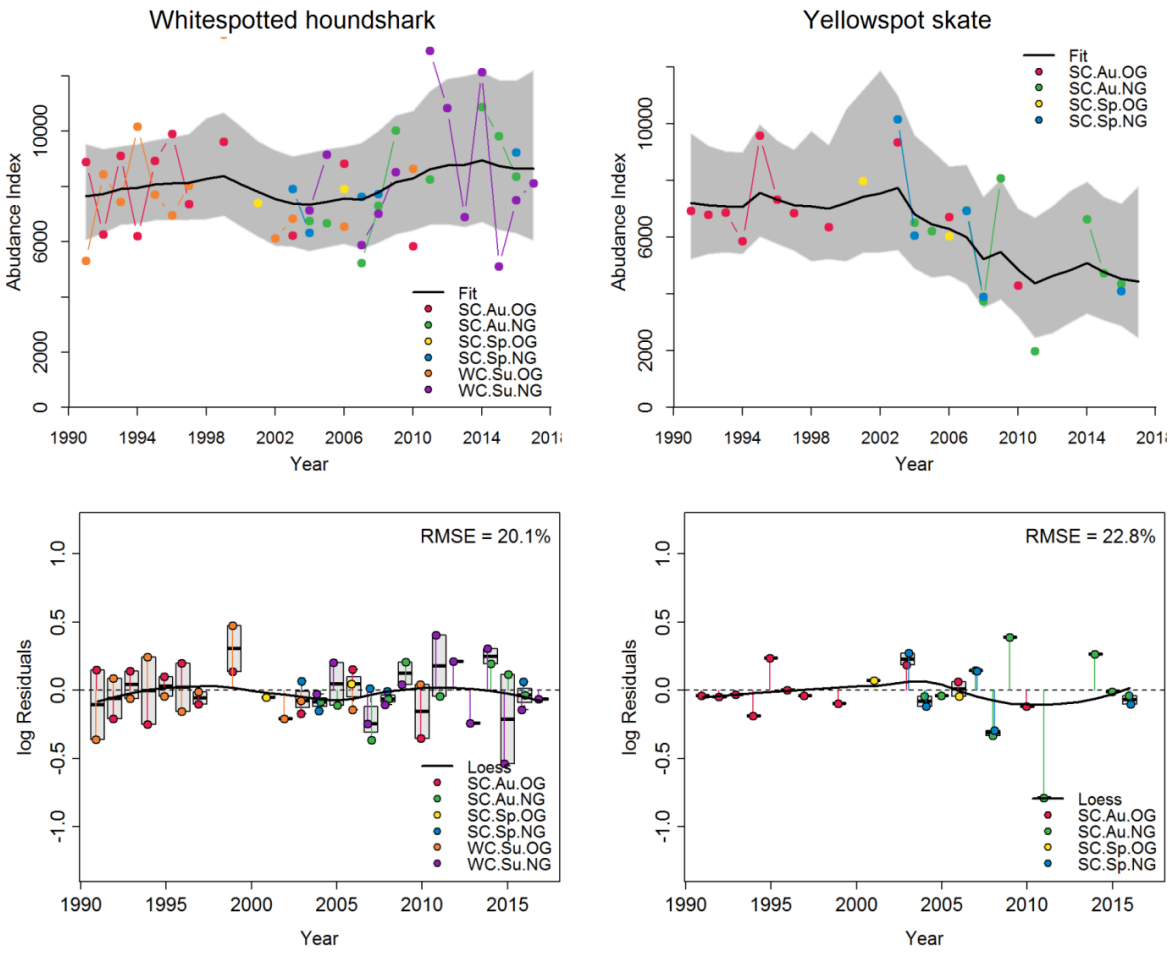

Figures 2: Model diagnostics plots produced by JARA using data from (left) Whitespot smoothhound *Mustelus palumbes* and (right) Yellowspotted Skate *Leucoraja wallacei*. Upper panel show observed relative abundance (coloured points) for each catch per unit effort (CPUE) timeseries, overall model fits (predicted relative abundance, black line) and 95% posterior predictive credibility intervals (grey polygons). Lower panel show colour-coded lognormal residuals of observed versus predicted abundance indices (coloured points), boxplots (grey bars) indicating the median and quantiles of all residuals available for any given year, and a loess smoother (black line) through all residuals to highlight any systematically auto-correlated residual patterns.

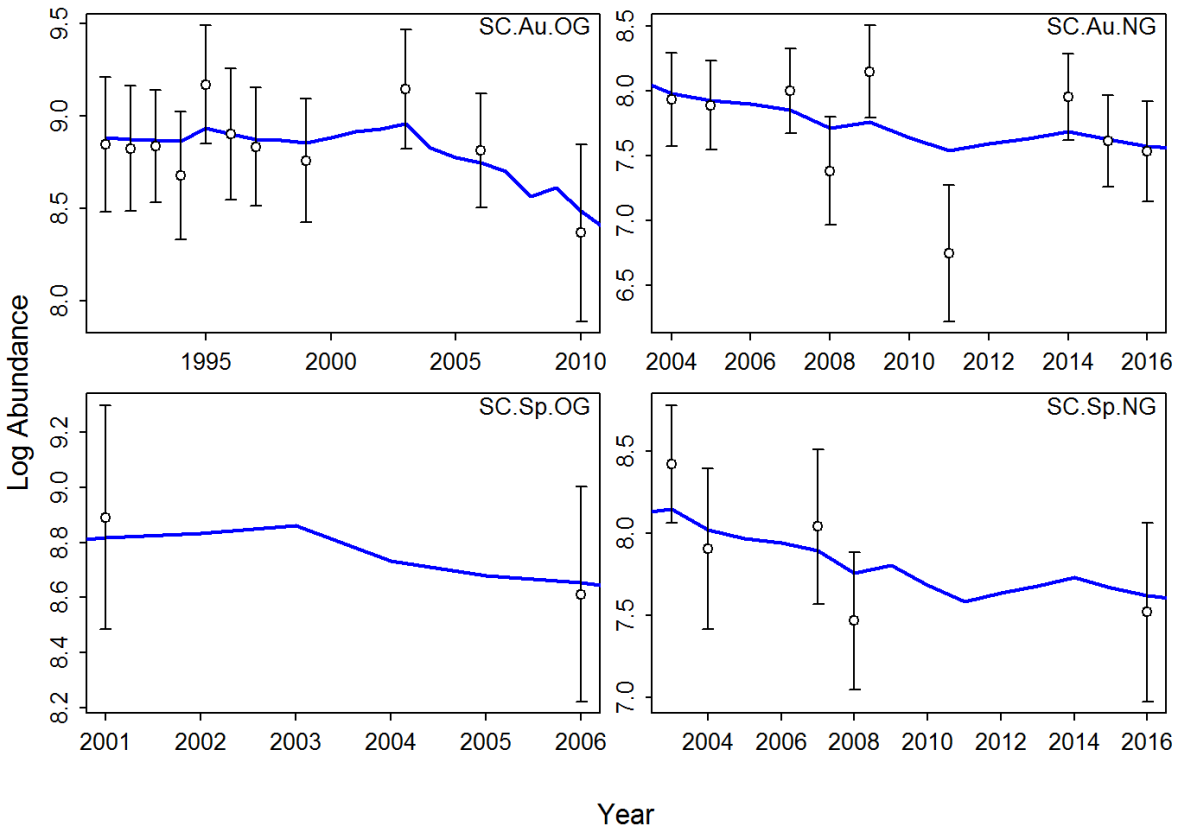

Figure 3: Model diagnostics plots produced by JARA using data from Yellowspotted Skate *Leucoraja wallacei*. Each panel shows the state-space model fit (blue line) to the natural logarithm (log) of the observed relative abundance data (white points), shown with 95% credible intervals (black lines) derived from the observation variance.

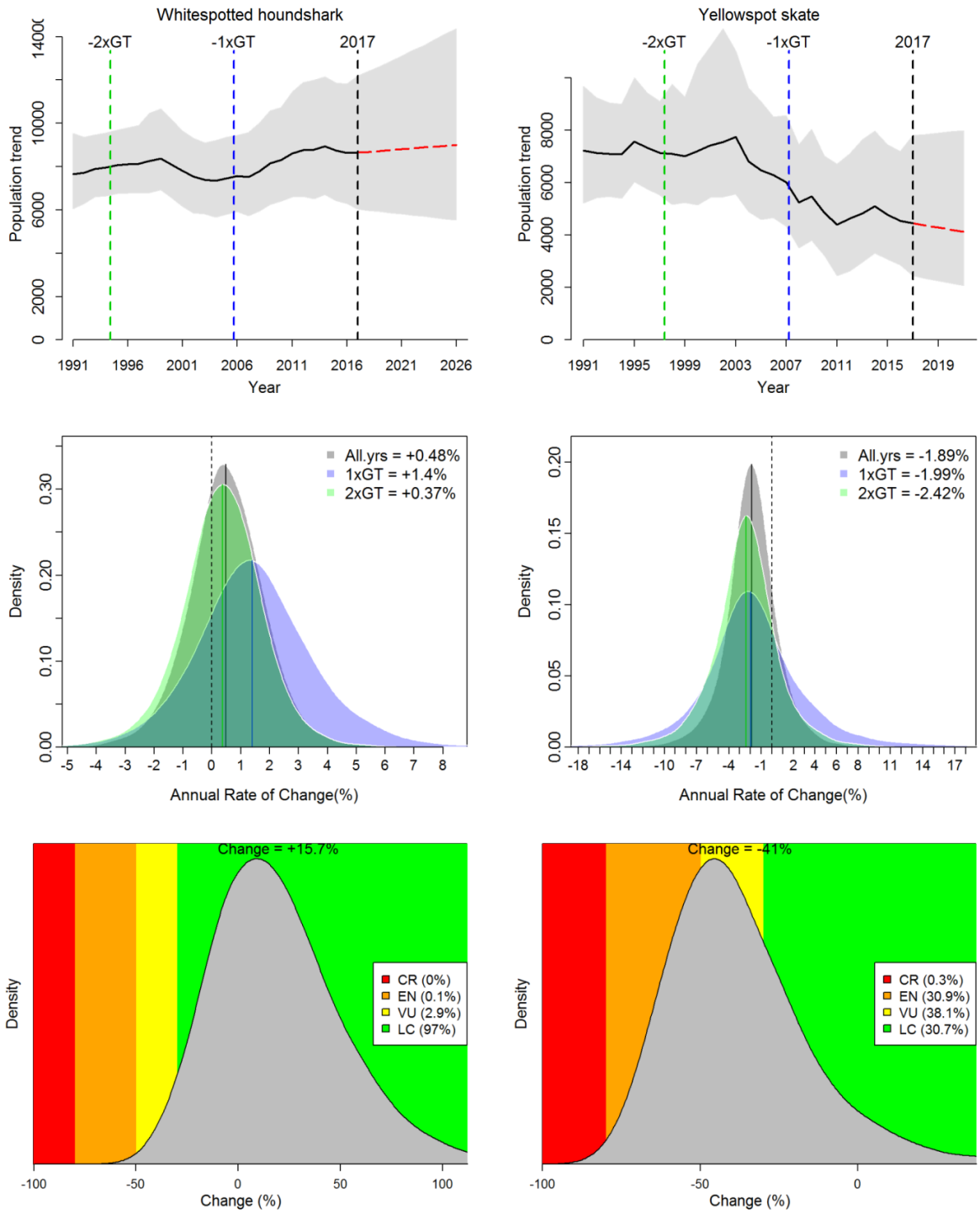

Figure 4: JARA decision-support plots for (left) Whitespot smoothhound *Mustelus palumbes* and (right) Yellowspotted Skate *Leucoraja wallacei* showing (top row) the overall JARA fit (black line) to the observed timeseries and the projected (red line) population trajectory over three generation times (GT); (middle row) the posterior probability for the percentage annual population change calculated from all the observed data (in black), from the last 1 generation length (in blue), from the last 2 generation lengths (in green) with the medians (solid lines) shown relative to a stable population (% change = 0, black dashed line); and (bottom row) the median change over

three generation lengths ("Change = xx") and corresponding probabilities for rates of population change falling within the IUCN Red List categories.

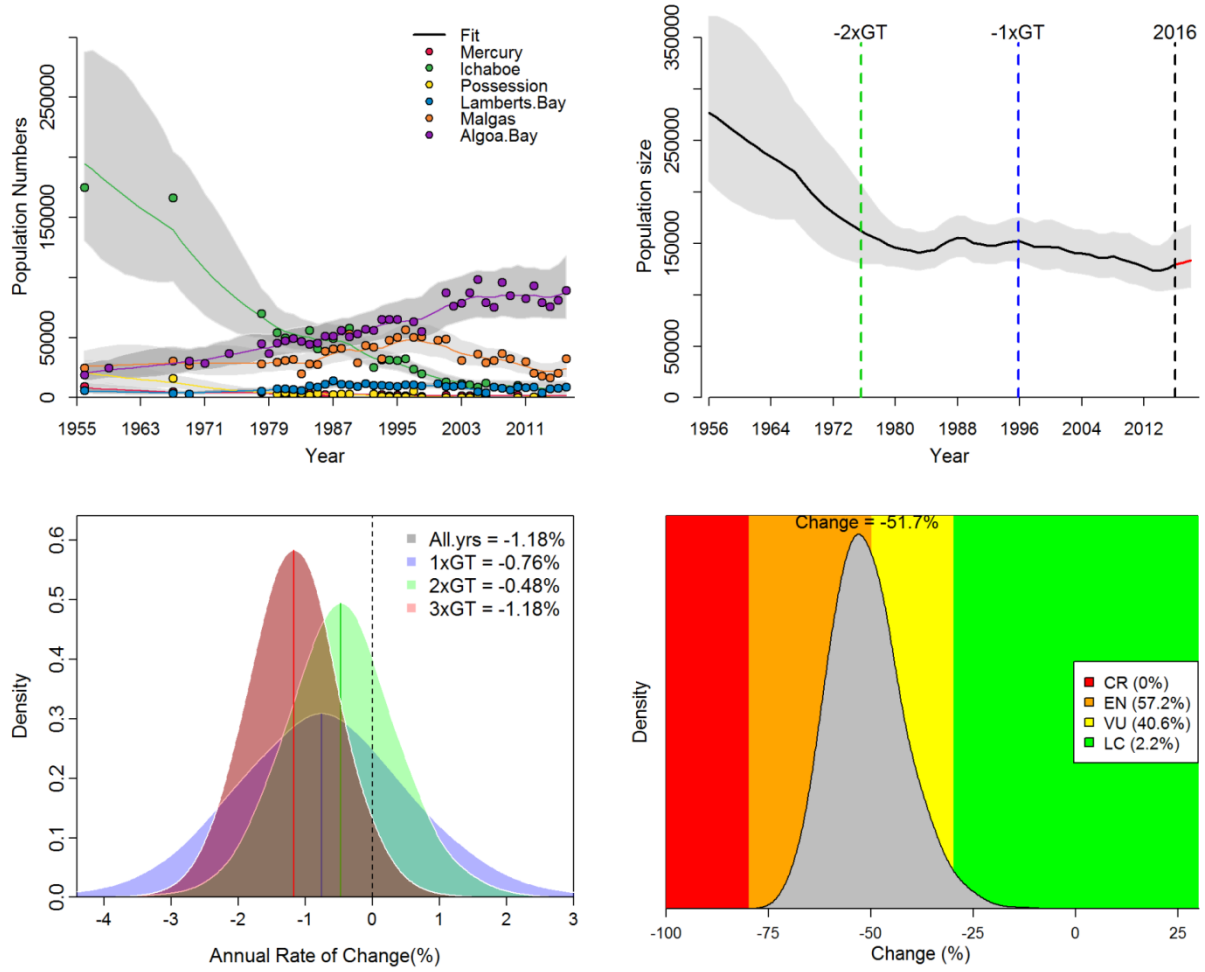

Figure 5: JARA decision-support plots for Cape Gannet *Morus capensis* showing (top left) the JARA fits (coloured lines) and 95% credible intervals (grey polygons) to each observed abundance timeseries (coloured points); (top right) the overall JARA fit (black line) to the observed timeseries and the projected (red line) population trajectory over three generation times (GT); (bottom left) the posterior probability for the percentage annual population change calculated from all the observed data (in black), from the last 1 generation length (in blue), from the last 2 generation lengths (in green), and from the last 3 generation lengths (in red) with the means (solid lines) shown relative to a stable population (% change = 0, black dashed line); and (bottom right) the median change over three generation lengths ("Change = xx") and corresponding probabilities for rates of population change falling within the IUCN Red List categories.

References

Akçakaya, T., Ferson, S., Burgman, M. A., Keith, D. A., Mace, G. M., Todd, C. R., … Ferson, S. (2000). Making consistent IUCN classifications under uncertainty. *Conservation Biology*, *14*(4), 1001–1013.

Bauer, H., Chapron, G., Nowell, K., Henschel, P., Funston, P., Hunter, L. T. B., … Packer, C. (2015). Lion (*Panthera leo*) populations are declining rapidly across Africa, except in intensively managed areas. *Proceedings of the National Academy of Sciences*, *112*(48), 14894–14899.

Boyd, C., DeMaster, D. P., Waples, R. S., Ward, E. J., & Taylor, B. L. (2017). Consistent Extinction Risk Assessment under the U.S. Endangered Species Act. *Conservation Letters*, *10*(3), 328–336.

Buckland, S. T., Newman, K. B., Thomas, L., & Koesters, N. B. (2004). State-space models for the dynamics of wild animal populations. *Ecological Modelling*, *171*(1–2), 157–175.

Butchart, S. H. M., Stattersfield, A. J., Bennun, L. A., Shutes, S. M., Akçakaya, H. R., Baillie, J. E. M., … Mace, G. M. (2004). Measuring global trends in the status of biodiversity: Red list indices for birds. *PLoS Biology*, *2*(12), e383.

Caughley, G. (1994). Directions in Conservation Biology. *Journal of Animal Ecology*, *63*(2), 215–244.

Connors, B. M., Cooper, A. B., Peterman, R. M., & Dulvy, N. K. (2014). The false classification of extinction risk in noisy environments. *Proceedings of the Royal Society B: Biological Sciences*, *281*, 20132935.

de Valpine, P., & Hastings, A. (2002). Fitting population models incorporating process noise and observation error. *Ecological Monographs*, *72*(1), 57–76.

Dulvy, N. K., Jennings, S., Rogers, S. I., & Maxwell, D. L. (2006). Threat and decline in fishes: an indicator of marine biodiversity. *Canadian Journal of Fisheries and Aquatic Sciences*, *63*(6), 1267–1275.

Fox, R., Harrower, C. A., Bell, J. R., Shortall, C. R., Middlebrook, I., & Wilson, R. J. (2018). Insect population trends and the IUCN Red List process. *Journal of Insect Conservation*, *23*(2), 269–278.

Hoffmann, M., Brooks, T. M., Da Fonseca, G. A. B., Gascon, C., Hawkins, A. F. A., James, R. E., … Silva, J. M. C. (2008). Conservation planning and the IUCN Red List. *Endangered Species Research*, *6*(2), 113–125.

IUCN. (2017). Guidelines for Using the IUCN Red List Categories and Criteria. Prepared by the Standards and Petitions Subcommittee. Retrieved from http://www.iucnredlist.org/documents/RedListGuidelines.pdf

Kery, M., & Schaub, M. (2012). *Bayesian Population Analysis using WinBUGS: A hierarchical perspective*. Waltham, MA: Academic Press.

Lee, C. K. F., Keith, D. A., Nicholson, E., & Murray, N. J. (2019). REDLISTR: Tools for the IUCN Red Lists of Ecosystems and Threatened Species in R. *Ecography*, *42(5)*, 1050–1055.

Mace, G. M., Collar, N. J., Gaston, K. J., Hilton-Taylor, C., Akçakaya, H. R., Leader-Williams, N., … Stuart, S. N. (2008). Quantification of extinction risk: IUCN's system for classifying threatened species. *Conservation Biology*, *22*(6), 1424–1442.

Regan, T. J., Taylor, B. L., Thompson, G. G., Cochrane, J. F., Ralls, K., Runge, M. C., & Merrick, R. (2013). Testing decision rules for categorizing species' extinction risk to help develop quantitative listing criteria for the U.S. endangered species act. *Conservation Biology*, *27*(4), 821–831.

Rueda-Cediel, P., Anderson, K. E., Regan, T. J., & Regan, H. M. (2018). Effects of uncertainty and variability on population declines and IUCN Red List classifications. *Conservation Biology*, *32*(4), 916–925.

Seminoff, J. A., & Shanker, K. (2008). Marine turtles and IUCN Red Listing: A review of the process, the pitfalls, and novel assessment approaches. *Journal of Experimental Marine Biology and Ecology*, *356*(1–2), 52–68.

Sherley, R. B., Barham, B. J., Barham, P. J., Campbell, K. J., Crawford, R. J. M., Grigg, J., … Votier, S. C. (2018). Bayesian inference reveals positive but subtle effects of experimental fishery closures on marine predator demographics. *Proceedings of the Royal Society of London, Series B: Biological Sciences*, *285*, 20172443.

Simmons, R. E., Kolberg, H., Braby, R., & Erni, B. (2015). Declines in migrant shorebird populations from a winter-quarter perspective. *Conservation Biology*, *29*(3), 877–887.

Thorson, J. T., & Minto, C. (2015). Mixed effects: a unifying framework for statistical modelling in fisheries biology. *ICES Journal of Marine Science*, *72*(5), 1245–1256.

Wilson, H. B., Kendall, B. E., & Possingham, H. P. (2011). Variability in Population Abundance and the Classification of Extinction Risk. *Conservation Biology*, *25*(4), 747–757.

Winker, H., Carvalho, F., & Kapur, M. (2018). JABBA: Just Another Bayesian Biomass Assessment. *Fisheries Research*, *204*, 275–288.